OPEN ACCESS

University of BRISTOL

Peer reviewed version

Link to published version (if available):
10.1061/(ASCE)GT.1943-5606.0001312

Link to publication record in Explore Bristol Research
PDF-document

University of Bristol - Explore Bristol Research
General rights

1   **Kinematic Framework for Evaluating Seismic Earth Pressures on Retaining Walls**

2   by

3   Scott J. Brandenberg[1], **M. ASCE**, George Mylonakis[2], **M. ASCE**, and Jonathan P. Stewart[3], **F. ASCE**

4   **Abstract:** During earthquake ground shaking earth pressures on retaining structures can

5   cyclically increase and decrease as a result of inertial forces applied to the walls and kinematic

6   interactions between the stiff wall elements and surrounding soil. The application, based on limit

7   equilibrium analysis, of a pseudo-static inertial force to a soil wedge behind the wall (the

8   mechanism behind the widely-used Mononobe-Okabe method) is a poor analogy for either

9   inertial or kinematic wall-soil interaction. This paper demonstrates that the kinematic component

10   of interaction varies strongly with the ratio of wavelength to wall height (λ/H), asymptotically

11   approaching zero for large λ/H, and oscillating between the peak value and zero for $\lambda/H < 2.3$.

12   Base compliance, represented in the form of translational and rotational stiffness, reduces

13   seismic earth pressure by permitting the walls to conform more closely to the free-field soil

14   displacement profile. This framework can explain both relatively low seismic pressures observed

15   in recent experiments with $\lambda/H > \sim 10$, and relatively high seismic earth pressures from numerical

16   analyses in the literature with $\lambda/H = 4$.

17   **Keywords:** wall, seismic earth pressure, wave, analysis, dynamic testing

18

[1] Associate Professor and Vice Chair, Department of Civil and Environmental Engineering, 5731 Boelter Hall, University of California, Los Angeles, CA 90095-1593. Email: sjbrandenberg@ucla.edu.
[2] Professor and Chair in Geotechnics and Soil-Structure Interaction, Department of Civil Engineering, University Walk, Clifton BS8, University of Bristol, UK; Professor, University of Patras, Greece; Adjunct Professor, University of California, Los Angeles. Email: g.mylonakis@bristol.ac.uk.
[3] Professor and Chair, Department of Civil and Environmental Engineering, 5731 Boelter Hall, University of California, Los Angeles, CA 90095-1593. Email: jstewart@seas.ucla.edu.

Introduction

The increment of lateral earth pressure that should be applied during the design of retaining walls to account for earthquake effects has been a source of confusion among design professionals and a topic on which there are divergent opinions among researchers. Current guidelines documents (*e.g.*, NCHRP, 2008) prescribe substantial seismic earth pressures beyond those for the pre-seismic (generally active) condition. These recommendations are based on a limit equilibrium analysis in which a pseudo-static seismic coefficient (k_h) acts upon an active Coulomb-type wedge in frictional soil, which in turn results in an incremental change in the lateral force applied to the wall, P_{AE}, over its static counterpart P_A. This approach is based on the classical work by Okabe (1924) and Mononobe and Matsuo (1929) [widely known as the "Mononobe-Okabe" (M-O) method] with modest modification by Seed and Whitman (1970). More accurate variants on the classical approach using non-planar failure surfaces (Chen, 1975; Chen and Liu, 1990) and approximate accounting for the phasing of inertial demands within the wedge (Steedman and Zeng, 1990) are conceptually alike and provide similar results for the active case.

Recent work based on experiments and various dynamic solutions considering elastic soil behavior has, directly or indirectly, challenged this practice as being both too conservative (e.g., Al Atik and Sitar, 2010; Lew et al., 2010) and as being un-conservative (e.g., Wood 1973, Veletsos and Younan 1994, Ostadan, 2005). These conflicting findings, based on different approaches and assumptions regarding system behavior, drive a good deal of the confusion on the subject of seismic earth pressures on retaining walls. A fundamental problem is that the M-O method does not adequately represent interaction of vibrating soil in the free field with an embedded structure or a retaining wall. This interaction may be best understood using a

41   conceptual framework, rooted in the principles of soil-structure interaction and wave

42   propagation, in which kinematic and inertial interaction effects are distinguished.

43   The next section describes a conceptual framework for defining seismic earth pressures from

44   kinematic interaction in terms of the ratio of wavelength of vertically propagating shear waves to

45   wall height. This approach convincingly explains the apparently divergent findings from

46   centrifuge tests by Al Atik and Sitar (2010) and the numerical results from Ostadan (2005).

47   Recommendations for rational simplified analysis of seismic earth pressures in engineering

48   practice are then presented, along with conditions for which more elaborate analyses are needed.

49   **Conceptual Framework**

50   The seismic increment to lateral earth pressures can be considered as having kinematic and

51   inertial components, as illustrated in Figure 1 for an embedded building foundation with

52   relatively stiff basement walls. The free-field motion imposed on this system (u_g) varies with

53   depth as indicated in Figure 1(a). In the kinematic problem for which there is no structure or wall

54   inertia, the motion of the foundation at base depth H is denoted u_{FIM} (FIM is "foundation input

55   motion"), which differs from the free-field motion at this same depth, $u_g(H)$, as a result of

56   relative foundation/free-field displacements associated with wall-soil contact stresses, as well as

57   base slab averaging effects that occur in the presence of inclined or incoherent waves (e.g.,

58   Veletsos and Prasad, 1989). The kinematic component of seismic earth pressures accounts for

59   the interaction between the free-field motion $u_g(z)$ and the structural wall elements, apart from

60   their inertia and any external inertial loads imposed upon the system.

61   As shown in Figure 1(b), the inertial interaction problem involves computation of the response of

62   a structure and its foundation to the kinematic ground motions. Inertial forces from the structure

63   cause additional relative displacements between the foundation and the free-field, and additional

64   increments of seismic earth pressure. The springs and dashpots in Figure 1(b) represent the

65   impedance of the foundation from translation and rocking vibration modes (*e.g.,* Pais and

66   Kausel, 1988; Gazetas, 1991).

67   In light of the above soil-structure interaction framework, the soil wedge concept currently used

68   to evaluate seismic earth pressures will seldom have relevance to the physical mechanisms

69   producing those pressures. Even in cases where a state of active earth pressure (and its associated

70   soil wedge) exists prior to seismic shaking, increments of earth pressure from earthquake ground

71   shaking will arise from relative displacements between the wall and free-field soil associated

72   with kinematic and inertial interaction, which is not well represented by a seismic coefficient

73   acting on an active wedge. Inertial interaction can mobilize large relative displacements when,

74   for example, a massive structure is connected to the wall elements and base shear mobilizes

75   reaction stresses at the soil/wall interface. Such effects can be evaluated as part of seismic

76   structural response analysis if soil springs are included in the structural model. Free-standing

77   walls or basement walls not structurally connected to lateral force resisting elements in structures

78   would have seismic earth pressures dominated by kinematic interaction, which is the topic

79   addressed in the remainder of this article.

80   **Model Derivation**

81   Seismic earth pressures arising from kinematic interaction are formulated based on the following

82   assumptions (Fig. 2): (1) an infinitely long U-shaped structure with rigid walls and rigid base

83   slab is embedded in a soil profile with a uniform shear wave velocity, (2) a vertically

84   propagating shear wave interacts with the embedded structure, (3) the soil and wall are in perfect

85   contact, and a gap does not form at this interface, and (4) the interaction between the soil and

86   vertical walls is characterized by stiffness intensity terms, k_y^i and k_z^i (defined below), and

87   interaction between the soil and base slab is characterized by stiffness terms K_y and $K_{xx,base}$.

88   These stiffness terms satisfy the Winkler assumption that the stiffness values act independently

89   from one another, which is a simplifying assumption commonly used in soil-structure interaction

90   problems because it permits development of tractable solutions. The values assigned to the

91   stiffness terms should account for coupling between various foundation vibrations modes, as

92   described later. Although these assumptions may appear to be limiting, the method can be readily

93   extended to a wide range of practical conditions (including non-rigid foundations as well as non-

94   linear and non-uniform soil) in a manner typical of soil-structure interaction applications (NIST,

95   2012) as illustrated subsequently.

96   The model derivation is described in two stages. *First*, wall pressures and their resultant demands

97   (forces and moments) are derived from the product of differential wall/free-field displacement

98   and wall-soil stiffness. *Second*, equations for the stiffness terms are developed, which is essential

99   for analysis of force/moment demands and differential wall/free-field motions. Fundamental

100   characteristics of wall-soil interaction derived from these analyses are then described and

101   illustrated using example solutions, which demonstrate that the wall-soil interaction response

102   depends strongly on the ratio of wavelength to wall height.

103   Wall-Soil Interaction Forces and Displacements

104   A rigid U-shaped structure with vertical walls embedded in a soil profile experiencing vertically

105   propagating harmonic free-field shear waves is shown in Figure 2. Note that the free-field

106   ground motion is consistent with the influence of the free-surface since the shear strain is zero at

107    $z=0$.

108   Kinematic wall pressures arise from incompatibility in the displacement of the rigid wall and the

109   free-field soil column. Accordingly, the integral of the horizontal stress increment over the

110   height of the wall is the kinematic seismic force increment P_E (P_E is adopted here instead of P_{AE},

111   which is associated with M-O theory, because our solution does not require an active condition).

112   For ground motion in the y-direction, P_E is calculated as a force per unit length as follows:

$$P_E = \int_0^H k_y^i \left(u_{g0} \cos kz - u_w(z) \right) dz \tag{1}$$

114   where H = wall height, $u_w(z)$ = wall displacement at depth z, k_y^i = soil-wall reaction stiffness in

115   y-direction (normal stresses) per unit of wall area (superscript i denotes stiffness intensity

116   measured in units of F/L^3; details below), $k=2\pi/\lambda$ = wave number, and λ = wavelength of the

117   shear wave propagating vertically through the soil. The moment applied by the horizontal soil-

118   wall interaction stresses relative to the foundation slab base elevation is:

$$M_E = \int_0^H k_y^i (H-z) \left(u_{g0} \cos kz - u_w(z) \right) dz \tag{2}$$

120   Equations (1) and (2) can be combined to calculate the location of resultant P_E, measured as

121   distance h upwards from the base of the wall as:

$$\frac{h}{H} = \frac{M_E}{P_E H} \tag{3}$$

123   The depth-dependent wall displacement $u_w(z)$ for a rigid wall and foundation system is:

124
$$u_w(z) = u_{FIM} + \theta_{FIM}(H - z) \qquad (4)$$

125 where u_{FIM} and θ_{FIM} are the base slab translation and rotation, respectively.

126 For a rigid wall resting on a rigid base, θ_{FIM} must be zero, base displacement must equal free-

127 field displacement at the base of the wall (i.e., $u_{FIM} = u_{g0}\cos kH$), and the solution for P_E, and M_E

128 may easily be obtained from Eqs. 1 and 2 for a free-field ground motion with any particular

129 wavelength. However, a more general solution for a wall embedded within an elastic layer,

130 thereby exhibiting base compliance, can also be obtained. The rotational stiffness of the

131 embedded strip contains contributions from the base slab and from vertical shear tractions and

132 horizontal normal stresses acting on the walls. The horizontal stresses acting on the walls are

133 explicitly included in Eqs. (1) and (2). The base slab and vertical traction contributions are

134 combined as $K_{xx} = K_{xx,base} + 2k_z^i HB^2$.

135 To solve for the foundation input motions, horizontal force and moment equilibrium of the

136 foundation slab are considered, assuming that the free-field ground motion is input to the free-

137 ends of the soil-structure interaction elements. Substituting (4) into (1) and (2), and requiring

138 horizontal force and moment equilibrium between the wall resultants and base reactions

139 provides:

140
$$P_E = \int_0^H k_y^i \left[u_{g0}\cos kz - u_{FIM} - \theta_{FIM}(H - z) \right] dz = \frac{K_y}{2}\left[u_{FIM} - u_{g0}\cos kH \right] \qquad (5a)$$

141
$$M_E = \int_0^H k_y^i \left[u_{g0}\cos kz - u_{FIM} - \theta_{FIM}(H - z) \right](H - z)\,dz = \frac{K_{xx}\theta_{FIM}}{2} \qquad (5b)$$

142 Stiffness terms K_y and K_{xx} are multiplied by ½ to account for two vertical walls being attached to

143 a single rigid base. By evaluating the integrals and re-arranging terms, the following solution is

144 obtained for foundation displacements:

145 $$H_u = \frac{u_{FIM}}{u_{g0}} = \frac{\left(6H^2\left(k_y^i\right)^2 + 3k^2 K_y K_{xx} + 2k^2 H^3 K_y k_y^i\right)\cos kH + \left(4kH^3\left(k_y^i\right)^2 + 6kK_{xx}k_y^i\right)\sin kH - 6H^2\left(k_y^i\right)^2}{k^2\left(H^4\left(k_y^i\right)^2 + 2H^3 K_y k_y^i + 6HK_{xx}k_y^i + 3K_y K_{xx}\right)}$$

146   (6a)

147 $$H_\theta = \frac{\theta_{FIM}B}{u_{g0}} = B\frac{\left(6k^2 H^2 K_y k_y^i + 24H\left(k_y^i\right)^2 + 12K_y k_y^i\right)\sin^2(kH/2) - 6kH^2\left(k_y^i\right)^2 \sin kH - 3H^2 k^2 K_y k_y^i}{k^2\left(H^4\left(k_y^i\right)^2 + 2H^3 K_y k_y^i + 6HK_{xx}k_y^i + 3K_y K_{xx}\right)}$$

148   (6b)

149 These foundation displacements can then be inserted into Eq. (5) to obtain P_E and M_E for a

150 compliant base condition.

151 <u>Stiffness of Wall-Soil System</u>

152 Having formulated the solution for P_E and M_E, the stiffness terms, k_y^i, k_z^i, K_y, and $K_{xx,base}$, are now

153 evaluated. Classical inertial SSI literature (e.g., summarized by Gazetas 1983, Mylonakis et al.

154 2006, and NIST 2012) provides equations for the overall stiffness of embedded foundations

155 representing the interaction of the soil with the entire foundation system, but the global stiffness

156 is not partitioned into contributions from the vertical walls and the base slab. Such partitioning is

157 required to obtain the distribution of earth pressure acting on the vertical walls, which is the

158 objective. To overcome this problem, available solutions are first used to define stiffness terms

159 for individual foundation components under the assumption of no interaction between vibration

160 modes (i.e., the components are independent). Next, modification factors χ_y and χ_{xx} are

161 introduced to account for interaction between the translation and rotation terms, respectively,

162   such that the resulting global foundation stiffness matches published equations for embedded

163   foundations. For simplicity, the base and wall stiffnesses are both modified by the same χ_y and

164   χ_{xx} terms.

165   *Horizontal wall-soil stiffness intensity k_y^i*

166   Kloukinas et al. (2012) developed a simple analytical expression for k_y^i for kinematic interaction

167   between rigid vertical walls and an elastic soil layer resting atop a rigid base. Following

168   correction of their published expression (a clerical error involving omission of the square root in

169   the denominator) and including the multiplier, χ_y, we obtain the stiffness intensity as:

170    $$k_y^i = \chi_y \frac{\pi}{\sqrt{(1-v)(2-v)}} \frac{G}{H} \sqrt{1 - \left(\frac{2\omega H}{\pi V_s}\right)^2}$$ (7a)

171   where ω is angular frequency (rad/sec). Material damping can be incorporated into the solution

172   by using complex shear modulus, $G(1+\mathbf{i}2\xi)$, and complex shear wave velocity, $V_s(1+\mathbf{i}\xi)$, where ξ

173   is percent material damping. Kloukinas et al. (2012) develop kinematic earth pressures for a rigid

174   wall resting atop a rigid base, whereas our solution corresponds to soil profiles that are deeper

175   and compliant under the wall, which is applicable to more realistic conditions. For an ideally

176   undamped medium, the square root on the right-hand side of Eq. (7a) can be interpreted as a

177   dynamic stiffness modifier (often denoted by α) that accounts for frequency-dependence from

178   soil inertia, with the corresponding dashpot equal to zero. At $\omega = \pi V_s / 2H$ the dynamic modifier

179   becomes zero and at higher frequencies k_y^i becomes imaginary meaning that the spring acts as a

180   dashpot. This phenomenon is directly related to the rigid base condition used in the solution,

181   which only allows radiation damping (from wave propagation away from the foundation) beyond

182   the "cutoff frequency" (e.g., Elsabee and Morray, 1977). For realistic systems involving a

183   compliant base condition, the cutoff frequency transition is smoother, allowing waves to exist at

184   a wider range of frequencies (Li, 1999), and material damping results in non-zero real and

185   imaginary components at all frequencies. Elsabee and Morray (1977) suggest simple expressions

186   for handling these problems for embedded circular foundations, but there is presently no simple

187   solution analogous to Eq. (7a) to account for these effects for two-dimensional vertical walls.

188   *Vertical wall-soil stiffness intensity k_z^i*

189   Following the method of Kloukinas et al. (2012), the digital supplement presents the derivation

190   of an expression for stiffness intensity associated with vertical tractions acting on walls (soil-wall

191   reaction stiffness in z-direction from shear), k_z^i. The resulting expression is given below along

192   with a multiplier, χ_{xx}, that modifies the vertical stiffness to account for interaction associated

193   with base rotation and translation:

194    $$k_z^i = \chi_{xx} \frac{\pi}{2} \sqrt{\frac{2-v}{1-v}} \frac{G}{H} \sqrt{1 - \left(\frac{2\omega H}{\pi V_s}\right)^2}$$ (7b)

195   *Base slab stiffness terms K_y and $K_{xx,base}$*

196   Gazetas and Roesset (1976) developed simple analytical expressions for the translational and

197   rotational stiffness (K_y and $K_{xx,base}$, respectively) of a rigid strip footing resting on the surface of a

198   homogeneous elastic layer of finite thickness overlying a rigid base. Applying the interaction

199   constants χ_y and χ_{xx} and adjusting the soil thickness term to be equal to the distance from the

200   base slab to the rigid base (i.e., using D-H), results in:

201 $$K_y = \chi_y \frac{2.1G}{2-\nu}\left(1+2\frac{B}{D-H}\right), \quad K_{xx,base} = \chi_{xx} \frac{\pi G B^2}{2(1-\nu)}\left(1+\frac{1}{5}\frac{B}{D-H}\right) \qquad \text{(8a, 8b)}$$

202 It should be noted that the solution in Eq. (8a) does not extrapolate properly to an infinitely thick

203 elastic layer, for which the stiffness of a strip footing is zero. On the other hand, under such a

204 condition the solution in Eq. (8b) is exact (Mushkelishvili, 1963).

205 *Derivation of interaction terms χ_y and χ_{xx}*

206 The above component stiffnesses can be combined to compute overall static stiffnesses for the

207 embedded wall-soil system in translation and rocking. For translation, the stiffness is $2k_y^i H + K_y$,

208 which includes contributions from the vertical walls and the base slab. For rotation, the stiffness

209 is $k_y^i H^2 + K_{xx,base} + 2k_z^i H B^2$, which includes contributions from horizontal and vertical earth

210 pressures acting on the vertical walls and the rotational stiffness of the base slab.

211 Values of χ_y and χ_{xx} were selected such that the global stiffness of the foundation matches the

212 equations for embedded strip footings by Jakub and Roesset (1977):

213 $$K_{y\_emb} = \frac{2.1G}{2-\nu}\left(1+2\frac{B}{D}\right)\left(1+\frac{1}{3}\frac{H}{B}\right)\left(1+\frac{4}{3}\frac{H}{D}\right) = 2k_y^i H + K_y \qquad \text{(9a)}$$

214 $$K_{xx\_emb} = \frac{\pi G B^2}{2(1-\nu)}\left(1+\frac{1}{5}\frac{B}{D}\right)\left(1+\frac{H}{B}\right)\left(1+\frac{2}{3}\frac{H}{D}\right) = k_y^i H^2 + K_{xx,base} + 2k_z^i H B^2 \qquad \text{(9b)}$$

215 Expressions for χ_y and χ_{xx} can be obtained by substituting Eqs. (7) and (8) into (9). Figure 3

216 presents the values of χ_y and χ_{xx} versus H/B for various values of D/H. The solutions by Jakub

217 and Roesset are intended for conditions in which D/B > 2 and H/B < 2/3, and may provide

218 erroneous results for conditions outside these bounds. Extrapolation is bounded by the Kloukinas

219   et al. (2012) solution for $D/H=1$, in which case $\chi_y = 1.0$, and the halfspace solution when $D/H \rightarrow$

220   ∞, in which case $\chi_y = 0.0$. These bounds are presented in Fig. 3, and interpolation from the figure

221   is recommended for $D/H<2$ and $D/H>20$ rather than the values of χ_y and χ_{xx} implied by Eqs. (7)-

222   (9).

Characteristics of Wall-Soil Interaction Response

224   Figure 4 shows solutions for P_E computed using Eq. (5a) with the expression for foundation

225   input motion given in Eqs. (6). Results are plotted for various values of $K_y/(k_y^i H)$ and

226    $K_{xx}/(k_y^i H^2/3)$ (representing the relative contributions of the base slab and horizontal normal

227   stresses acting on the walls to horizontal and rotational stiffness, respectively). In addition to the

228   cases with a compliant base, a rigid base case (K_y and $K_{xx} \rightarrow \infty$) is included for comparison. For a

229   given λ/H, the highest values of P_E occur for the rigid base case. P_E decreases as K_y and K_{xx}

230   decrease because a more flexible base condition results in less relative displacement between the

231   wall and free-field soil along the wall height.

232   The most important interval of λ/H in Figure 4 for application to typical structural configurations

233   and earthquake ground motions is the portion to the right of the longest wavelength (lowest

234   frequency) peak in P_E, which occurs at $\lambda/H \approx 2.3$. The importance of this interval stems from its

235   likely proximity to energetic portions of the ground motion spectrum, which occur at the site

236   resonant frequency or at frequencies controlled by the seismic source and path (which are

237   typically higher than the site frequency for sites in sedimentary basins).

238   To support the assertion that the important portion of the plot is typically $\lambda/H \geq 2.3$, consider

239   first the case of free field seismic energy that is dominated by site resonance. The site resonant

240   frequency corresponds to $\lambda/D = 4$, which can be manipulated to $\lambda/H=4D/H$. Since the thickness

241   of the soil column generally significantly exceeds the wall height (i.e., generally $D \gg H$), λ/H will

242   typically exceed 4, which falls well to the right of the lowest frequency peak at $\lambda/H \geq 2.3$. For

243   this resonant condition, the largest kinematic pressures occur when $D=H$ (i.e., base slab is

244   founded on stiff rock overlain by soil).

245   Free-field ground motions are often not dominated by a fundamental-mode site response,

246   particularly in sedimentary basins where seismic velocities gradually increase with depth without

247   having a distinct impedance contrast. In such cases, the controlling ground motion period can be

248   estimated as the mean period (T_m = period at the centroid of the Fourier amplitude spectrum),

249   which is typically in the range of 0.3 to 0.5 sec for earthquakes in active crustal regions in the

250   magnitude range of engineering interest (Rathje, et al., 2004). The corresponding wavelenths

251   (computed as $\lambda = V_s T_m$) will seldom place the applicable value of λ/H below the peak at ~2.3 for

252   typical values of wall height H.

253   Based on the above considerations, the most useful insights into kinematic wall pressures are

254   gained by studying the portion of the results in Figure 4 for $\lambda/H > \sim 2.3$. Kinematic pressures are

255   clearly high near the peak at 2.3 due to large relative deformations of wall and soil. As λ/H

256   increases beyond 2.3, P_E decreases rapidly. In the limiting case where $\lambda/H \rightarrow \infty$, the deformed

257   shape of the free-field soil profile would become vertical and would precisely conform to the

258   shape of the rigid wall, thereby resulting in zero kinematic interaction. The peaks and troughs in

259   P_E observed for $\lambda/H < 2.3$ are caused by alternation of the direction of the horizontal stress

260   increment acting along the wall height as frequency changes.

261   Figure 5 shows kinematic transfer functions H_u and H_θ associated with the solution for the

262   foundation input motion (Eq. 6). The transfer functions are compared to the recommendation by

263   Kausel et al. (1978), who used an embedded cylinder geometry, assumed $u_{FIM} = u_g(H)$ (this is the

264   same as assuming $K_y \rightarrow \infty$), and approximated high frequency interaction (i.e., at low λ/H) as

265   constant with respect to frequency for simplicity. At large λ/H, the H_u values for the rigid base

266   case agree perfectly with Kausel et al., whereas base compliance results in increased translation

267   and rotation. The assumption that $u_{FIM} = u_g(H)$ is approximate, even in the presence of vertically

268   propagating coherent waves, due to the wall-soil interaction force P_E that must be balanced by

269   deflection of the base slab. As H/B increases, translation amplitude decreases and rotational

270   amplitude increases for a particular λ/H.

271   **Recommended Methods of Implementation**

272   The solution for P_E in Eq. 5a is a function of wave number, k, and is therefore a function of

273   frequency. The dependence of P_E on frequency can be captured with two methods: (1) a

274   frequency-domain solution that takes as input a time-series of free-field ground surface

275   displacement $[u_{g0}(t)]$, or (2) a single-frequency solution that takes as input a particular free-field

276   displacement (u_{g0}) and a single frequency anticipated to dominate dynamic earth pressure

277   response. Both methods will be useful in design applications and are described below.

278   The frequency domain solution (FD solution) has the following steps:

279   *1)*   Compute the Fourier transform of the free-field ground displacement record, $\hat{u}_{g0}(\omega)$

280   using a fast Fourier transform algorithm.

281   *2)*   Compute frequency-dependent values of the stiffness parameters k_y^i, k_z^i, K_y, and $K_{xx,base}$

282   using Eqns. (7)-(9). Follow typical protocols (NIST, 2012) for selecting representative

283   shear moduli for use in these expressions, including averaging non-uniform shear-wave

284   velocities over appropriate depth ranges and using applicable levels of modulus reduction

285   for nonlinear problems (described further below). Alternative values for embedded

286   foundation stiffness to those given in Eqs. (9), as derived from site- and structure-specific

287   analysis or from alternate solutions in the literature, can be readily incorporated by

288   entering the computed values for K_{y_emb} and K_{xx_emb}. This could be particularly important

289   for foundation geometries that are not well approximated as plane strain for a particular

290   direction of shaking [e.g., rectangular foundations, for which impedance solutions are

291   available in Gazetas (1983), Mylonakis et al. (2006) and NIST (2012)]. Material damping

292   may also be incorporated through the use of complex-valued shear moduli as noted

293   above.

294   *3)*   Compute the Fourier coefficients of the frequency-dependent foundation input motions

295        $\hat{u}_{FIM}(\omega)$ and $\hat{\theta}_{FIM}(\omega)$ using Eqs. 6a and 6b. Note that $\hat{u}_{g0}(\omega)$ is substituted for u_{g0} in

296   these equations for the frequency domain solution.

297   *4)*   Compute the Fourier coefficients of the seismic earth pressure resultant, $\hat{P}_E(\omega)$, using

298   Eq. 5a. Note that $\hat{u}_{g0}(\omega)$, $\hat{u}_{FIM}(\omega)$ and $\hat{\theta}_{FIM}(\omega)$ are substituted for u_{g0}, u_{FIM}, and θ_{FIM},

299   respectively.

300   *5)*   Compute the time series of the seismic earth pressure resultant, $P_E(t)$ using the inverse

301   fast Fourier transform algorithm. Find the maximum value of this time series. The total

302   demand on the wall is the sum of P_E (at the location indicated by Eq. 3) and the resultant

303   of the initial earth pressure (typically at $z = 2H/3$).

304   Each of the frequency-domain displacements and forces given above is complex valued.

305   The single-frequency solution (SF solution) is as follows:

306   *i.*   Estimate the mean period (T_m) of the design earthquake ground motion. For projects

307   where ground motions are estimated using site-specific probabilistic seismic hazard

308   analysis followed by the selection of applicable accelerograms, the mean period can be

309   computed for each record using procedures given in Rathje et al. (2004). When such

310   accelerograms are unavailable, T_m can be computed from applicable ground motion

311   prediction equations (*e.g.*, Rathje et al., 2004), or in cases of sites having significant

312   impedance contrasts giving rise to strongly resonant responses, from the site period

313          $\left(T = 4H/V_s\right)$.

314   *ii.*   Compute k_y^i, k_z^i, K_y, and $K_{xx,base}$ using Eqns. (7)-(9) or alternate solutions as described in

315   Step (2) above. For many practical situations, static stiffnesses will suffice for these

316   quantities (zero frequency), although more precision is possible through consideration of

317   frequency dependence.

318 *iii.*   Use the results in Fig. 4, or a site-specific solution of Eq. (5), to evaluate the variation of

319   normalized P_E [i.e., $\left|P_E\right|/\left(u_{g0}k_y^i H\right)$] versus λ/H.

320 *iv.*   Compute λ/H, based on the mean period from Step *(i)* (*i.e.*, $\lambda/H = V_s T/H$), and compute

321   the associated normalized value of P_E. Kinematic interaction is anticipated to be

322   significant if the wall under consideration lies near the fundamental-mode peak response

323   region (i.e., $\lambda/H \approx 1.5$ to 4), and small in regions of lower frequency (e.g., $\lambda/H > \sim 10$).

324   *v.*   Estimate u_{g0} so that the dimensionless wall force from *(iv)* can be dimensionalized.

325   Ground motion amplitude u_{g0} should not be perceived as the peak ground displacement,

326   but rather as a displacement associated with the most energetic portion of the record.

327   Until more detailed validation exercises can be performed, u_{g0} should be taken as

328   PGV/ω_m, where PGV is the peak ground velocity in the free field and ω_m is the angular

329   mean frequency corresponding to the mean period from (1) ($\omega_m = 2\pi/T_m$). Energetic

330   portions of the ground motion spectrum are correlated with PGV (e.g., Akkar and Özen,

331   2005; Bommer and Alarcón, 2006).

332 *vi.*   The total demand on the retaining wall is computed from P_E and the resultant of the

333   initial earth pressure, as in the FD procedure.

334   Several important issues arise when selecting a representative shear wave velocity using either

335   the FD or SF solutions. First, shear wave velocity typically varies with depth due to pressure-

336   dependence of soil shear modulus and age. For computing k_y^i and k_z^i, the time-averaged shear

337   wave velocity (depth/travel time) for the depth interval from the ground surface to the bottom of

338   the wall should be used. For computing base stiffness terms, the time-averaged shear wave

339   velocity for the depth interval from $z = H$ to $H+B$ should be used, until more detailed

340   recommendations can be developed.

341   Second, strong ground motion induces shear strains that are large enough to reduce the secant

342   shear modulus in accordance with a modulus reduction curve. Failing to account for modulus

343   reduction may result in a significant over-prediction of earth pressure since the reduction in

344   secant shear modulus reduces k_y^i, k_z^i, K_y, and $K_{xx,base}$. A site-specific ground response analysis is

345   recommended to obtain values of strain-compatible shear modulus (and associated equivalent-

346   linear V_s). An alternative crude approach is to approximate the peak shear strain based on

347   PGV/V_s. Assuming the standing wave field in Fig. 2 varies in time according to $u_g(z,t) =$

348   $u_{g0}\cdot\cos(kz)\cdot e^{i\omega t}$, the ground surface velocity is $du_g(0,t)/dt = \dot{u}_{g0} = i\cdot\omega\cdot u_{g0}\cdot e^{i\omega t}$ and the shear strain

349   is $du_g/dz = -k\cdot u_{g0}\cdot\sin(kz)\cdot e^{i\omega t}$. Therefore the strain field is $du_g/dz = (\dot{u}_{g0}/V_s)\cdot i\cdot\sin(kz)$, the

350   amplitude of which is simply PGV/V_s. The imaginary number indicates that shear strain is 90°

351   out of phase with surface velocity. Furthermore, the maximum values of shear strain occur at the

352   "nodes" of the standing wave (i.e., at $kz = \pi/2 + n\pi$, where n is an integer greater than 0). For

353   more complicated conditions including soil layering and propagation of surface waves, shear

354   strain has been found to range from 0.2 to 1.7 times PGV/V_s, with 1.0 being a commonly used

355   value for horizontal-component ground motions (Trifunac et al., 1996; Brandenberg et al., 2009),

356   which provides an estimate of peak shear strain consistent with the assumed shape of the soil

357   displacement profile. This peak shear strain can then be converted to a representative uniform

358   strain by multiplying the peak shear strain by (**M**-1)/10, where **M** is moment magnitude (Idriss

359   and Sun, 1991). The equivalent uniform shear strain would then be used to compute a value of

360   G/G_{max} from a selected modulus reduction curve, from which reduced values of G and V_s can be

361   obtained for use in the analysis. This equivalent-linear procedure neglects local strains imposed

362   by the wall, and is reasonable for cases involving free-field ground strains smaller than about

363   1%. However, the procedure may become erroneous at larger strains corresponding to ground

364   failure. Free-standing retaining walls that rotate or translate significantly may mobilize such

365   large shear strains, but this will rarely be the case for stiff building basement walls.

366   The solution presented herein assumes perfect contact between the soil and the vertical walls. In

367   reality, a gap might form in cohesive soils at this interface if P_E is negative (i.e., the wall is

368   moving away from the soil) and its absolute value is larger than the initial earth pressure on the

369   wall. Gapping may theoretically cause pounding and additional stresses on the wall beyond those

370   considered here. However, it is likely that peak earth pressures will occur when P_E is positive

371   (i.e., when the free-field soil moves toward the wall), which is considered in the present analysis.

372   The efficacy of the proposed procedure is demonstrated in the following section and will be

373   tested further over time as additional experimental data become available.

Comparison to Experimental- and Simulation-Based Results in Literature

375   In this section, two prior studies that reached strongly divergent conclusions about the levels of

376   seismic earth pressures acting on retaining walls are interpreted using the proposed methodology.

377   In the first study, Ostadan (2005) performed elastic wave propagation analysis using a numerical

378   finite element code (SASSI; Lysmer et al. 1999) to investigate the kinematic interaction between

379   free-field site response and a massless embedded structure connected to a rigid base and fixed

380   against rotation. Ostadan concluded that M-O earth pressure theory significantly under-predicts

381   the mobilized earth pressures by factors ranging from 2 to 4 depending on ground motion

382   characteristics. In the second study, Al Atik and Sitar (2009) performed centrifuge modeling of

383   embedded U-shaped walls, and concluded that M-O theory significantly over-predicts measured

384   earth pressures. On the basis of their test results, they reported that dynamic earth pressures

385   driving flexural demands on the walls are negligible for peak horizontal surface accelerations

386   less than 0.4g.

387   <u>Ostadan (2005) Numerical Solution</u>

388   Ostadan (2005) input six broadband earthquake motions, scaled to a common peak horizontal

389   acceleration of 0.3g, to the base of an elastic soil layer with V_s = 305 m/s, H = 9.14m, mass

390   density ρ=2.06Mg/m^3, ν=1/3, and ξ=5%. The elastic layer rests atop a rigid base. This elastic

391   layer is the backfill behind a rigid wall also supported on the rigid base. The ground motions

392   generated substantial site response due both to the infinite impedance contrast (from the rigid

393   base) and significant energy in the input motions at the fundamental frequency of the backfill

394   (where λ/H=4).

395   Five of the free-field surface motions were obtained from Ostadan (*pers. communication*, 2013)

396   and used to compute $u_{g0}(t)$ by double-integrating the surface accelerations in time. Those free-

397   field motions were then applied using the proposed FD and SF solutions. Since the base of the

398   wall was rigidly connected to the ground, only the stiffness term k_y^i is needed in the solution, and

399   the frequency-dependent value was computed using Eq. (7a) with $\chi_y = 1$. Figure 6a compares

400   maximum earth pressures over the wall height from the FD solution relative to those obtained by

401   Ostadan (2005) for two of the ground motions (three are omitted for clarity in the figure). Table

402   1 presents the resultants of these distributions. The resultant forces are in good agreement, with

403   errors ranging from -10% to +12%.

404   In the SF solution, the surface displacement is computed as $u_{g0}=PGV{\cdot}T/2\pi$, where *PGV* is taken

405   from ground-surface motions, and period *T* is taken as $4H/V_s$ due to the strong impedance

406   contrast at the base of the soil layer. The agreement with Ostadan's solution is reasonable, but

407   not as good as the FD solution, with errors ranging from -12% to +57%. The Mononobe-Okabe

408   earth pressure resultant presented by Ostadan (160 kN/m for all of ground motions)

409   underpredicts the earth pressures in every case.

410   The conditions considered by Ostadan are nearly optimal for generating large kinematic wall

411   pressures (i.e., $\lambda/H = 4$, associated with first mode response of the backfill, lies near the peaks of

412   the curves in Fig. 4). Not surprisingly, such conditions cause the mobilized earth pressures to

413   exceed those from the M-O theory. Ostadan's results are broadly consistent with earlier findings

414   by Arias et al. (1981) and Veletsos and Younan (1994) obtained by analytical closed-form

415   solutions for similar configurations.

416   Al Atik and Sitar (2009, 2010) Experimental Results

417   Al Atik and Sitar (2009, 2010) performed centrifuge experiments on relatively rigid and flexible

418   U-shaped walls with prototype dimensions of H = 6.5 m and B = 5.3m embedded in a profile of

419   medium dense sand with thickness D = 19 m, and γ = 17 kN/m^3. The average small-strain shear

420   wave velocities given by Al Atik and Sitar were V_s = 170 m/s behind the walls and V_s = 260 m/s

421   for the depth interval from the base of the wall to the essentially rigid base of the container. The

422   FD and SF solutions are compared with results of experiments performed using motions denoted

423   Loma Prieta SC1, Loma Prieta SC2, and Kobe PI2.

424   For these experiments, u_{g0} was obtained by digitizing and double-integrating in time the plots of

425   free-field surface acceleration presented by Al Atik and Sitar (2009). These motions induced

426   nonlinear response in the sand, and measured shear strains and the interpreted modulus reduction

427   (G/G_{max}) curve by Al Atik and Sitar were used to estimate representative values of G/G_{max} =

428   0.28, 0.25, and 0.10 for the SC1, SC2, and PI2 ground motions, respectively. Comparisons

429   between computed (FD solution) and measured maximum earth pressures for the three digitized

430   ground motions are shown in Fig. 6 for SC2 and PI2 (SC1 omitted for clarity). Resultant forces

431   for all three motions are shown in Table 2. Resultant force errors range from -7% to +23% for

432   the FD solution and from +6% to +23% for the SF solution. Although the earth pressure

433   resultants are predicted quite well, the shape of the pressure distributions differ significantly,

434   with the reported distributions from measurements increasing linearly with depth and the

435   predicted distributions being approximately zero at the base of the wall and having their

436   maximum at the ground surface. This mismatch may result in part from the assumption of depth-

437   invariant k_y^i, whereas the shear modulus of sand in the centrifuge models increases with depth. A

438   more robust solution would utilize k_y^i values that increase with depth in accordance with the

439   variation in soil shear modulus, combined with a site response study that captures the influence

440   of these variations on the free-field displacement profile. We lacked the required data to perform

441   such an analysis. It should be noted that the modulus reduction was an important part of this

442   analysis; if taken as unity (linear soil) earth pressures are significantly over-predicted.

443   Mononobe-Okabe earth pressures presented by Al Atik and Sitar (2009) were computed using

444   the ground surface *PGA* and 0.65*PGA*. For consistency with the Ostadan (2005) comparisons,

445   the PGA-based M-O estimates are presented here. As shown in Table 2, the M-O pressure

446   resultants significantly exceed the measurements. It is helpful to visualize these results relative to

447   the diagrams in Figure 4. If the frequency content of the motions in the centrifuge model are

448   assumed to be dominated by site response above the essentially rigid base of the container, then

449    $\lambda = 4D$, which produces $\lambda/H=12$. This is well to the right of the peak, and therefore anticipated

450   soil pressures from kinematic interaction are quite small. Not surprisingly, those pressures fall

451   below the range of M-O pressures.

452   The results in Figure 6 and Table 1 compare results from the proposed analysis with maximum

453   kinematic earth pressure increments presented by Al Atik and Sitar (2009) (i.e., total earth

454   pressure minus initial static earth pressure minus the component from inertia of the wall mass).

455   However, Al Atik and Sitar (2009) indicate that the peak bending moments in the walls arose

456   from a combination of kinematic and inertia loading, and peak moments were out-of-phase with

457   peak kinematic earth pressures. The evaluation of these inertial effects is a straightforward

458 extension of the proposed methodology, but is not considered here for brevity and because

459 required data is unavailable.

460 <u>Effect of Dynamic Modifier on Lateral Wall-Soil Stiffness Terms</u>

461 Calculations of P_E presented above utilized frequency-dependent stiffness terms (Eqns. 7a and

462 7b) for both the FD and SF solutions. The calculations were repeated omitting the dynamic

463 component (i.e., setting $\omega = 0$). Setting the frequency modifiers to unity increased the computed

464 earth pressures by about 15 to 20% for the FD solution for both the Ostadan and Al Atik and

465 Sitar cases. This generally increases model misfit to the data from the literature. Using the SF

466 solution, comparable pressure increases for the Al Atik and Sitar case are observed, but $> 200\%$

467 increases are observed for the Ostadan case.

468 On the basis of these comparisons, until more advanced models for k_y^i and k_z^i can be developed

469 that account for soil layering, application of the frequency-dependent terms in Eq. (7a) and (7b)

470 is recommended when the interaction effects are strong (i.e., near the peak of the transfer

471 functions in Figure 4, or $\lambda/H \approx$ 1.5-5.0). Otherwise, for the common case of $\lambda/H > 5$,

472 implementation of the dynamic modifier appears to be helpful but not essential.

473

474 **Recommendations and Conclusions**

475 We present a kinematic soil-structure interaction approach that provides a unifying framework to

476 explain the lower-than-M-O seismic earth pressure increments observed by Al-Atik and Sitar

477 (2009, 2010) and the higher-than-M-O pressure increments computed by Ostadan (2005),

478 Veletsos and Younan (1994), and others. The approach is admittedly simplified in several

479 respects; in particular, the effects of wall and foundation inertia are not considered (consistent

480 with a kinematic assumption), the Winkler assumption is utilized, the single-frequency solution

481 significantly simplifies the broadband ground motion driving the kinematic demands, soil

482 nonlinearity can only be indirectly included using an equivalent-linear approximation, and

483 potential impacts of alternate initial gravity-induced stress conditions (e.g., active, at-rest) on the

484 seismic earth pressure increment are not considered. Despite those caveats, the approach is

485 physically sound and provides a clear basis for understanding the factors driving seismic earth

486 pressures for many practical retaining wall configurations. Additional experimental observations

487 and numerical simulations are needed to validate the procedure for ranges of ground motion

488 frequencies and wall configurations, evaluate the relative contributions of inertial effects, and to

489 formulate detailed recommendations for design application. Nevertheless, the proposed approach

490 produces estimates of seismic earth pressures that are significantly more accurate than M-O

491 theory.

492 Numerical simulations are warranted for cases where the assumptions associated with the

493 proposed method are expected to produce unacceptably large errors. Seismic earth pressures

494 from inertial interaction should also be considered in general application, and may be the only

495 significant source of seismic earth pressures when kinematic interaction is insignificant. Inertial

496 demands have different origins, and as such, may be out of phase with kinematic demands.

497   Inertia demands should be evaluated separately using a procedure like that shown in Fig. 1b and

498   described in detail elsewhere (e.g., NIST, 2012).

499   **Acknowledgments**

503   **References**

504   Akkar, S. and Özen, Ö. (2005). "Effect of peak ground velocity on deformation demands for

505   SDOF systems," *Earthquake Eng. Struct. Dyn.* 34 (13), 1551–1571.

506   Al Atik, L. and Sitar, N. (2009). "Experimental and analytical study of the seismic performance

507   of retaining structures." *Rpt. No. PEER-2008/104*, Pacific Earthquake Engineering Research

508   Center, UC Berkeley.

509   Al Atik, L. and Sitar, N. (2010). "Seismic earth pressures on cantilever retaining structures," *J.

510   Geotech. & Geoenv. Eng.*, ASCE, 136 (10), 1324-1333.

511   Arias A, Sanchez-Sesma, F.J., Ovando-Shelley, E. (1981). "A simplified elastic model for

512   seismic analysis of earth-retaining structures with limited displacements," *Proc. Int Conf. Recent

513   Adv in Geotech. Eqk. Eng. & Soil Dyn.*, S Prakash, editor. Univ. of Missouri, Rolla, Vol 1, 235-

514   240**.**

515   Bommer, J. J. and Alarcón, J. E. (2006). "The prediction and use of peak ground velocity," *J.

516   Earthquake Eng.,* 10 **(**1), 1–17.

517   Brandenberg, S.J., Coe, J., Nigbor, R.L., and Tanksley, K. (2009). "Different approaches for

518   estimating ground strains from pile driving vibrations at a buried archeological site." *J. Geotech.*

519   *Geoenviron. Eng.*, 135(8), 1101–1112.

520   Chen, W.F. (1975). *Limit analysis and soil plasticity. Developments in geotechnical engineering*.

521   Elsevier, Amsterdam, The Netherlands.

522   Chen, W.F, and Liu, X.L. (1990). *Limit analysis in soil mechanics*. Elsevier, Amsterdam, The

523   Netherlands.

524   Elsabee, F. and Morray, J.P. (1977). "Dynamic behavior of embedded foundations," Publication

525   No. R77-33, MIT, Cambridge, MA.

526   Gazetas, G. (1983). "Analysis of machine vibrations: state of the art," *Soil Dyn. Earthquake*

527   *Eng.,* 2(1), 2-42.

528   Gazetas, G. (1991). "Foundation vibrations," *Foundation Engineering Handbook*, 2nd Edition,

529   Chapter 15, H.-Y. Fang, ed., Chapman and Hall, New York, New York.

530   Gazetas, G., and Roesset, J.M. (1976). "Forced vibrations of strip footings on layered soils," in

531   *Methods of Structural Analysis*, National Structural Engineering Conference; August 22-25,

532   1976, Madison, WI, WE Saul and AH Peyrol (eds.), ASCE, Vol. 1, 115-131.

533   Idriss, I.M., and Sun, J. I. (1991). "User's manual for SHAKE91", Center for Geotechnical

534   Modeling, University of California, Davis, CA, 65 p.

535   Jakub, M., and Roesset, J.M. (1977). "Nonlinear stiffness of foundations." *Research Report R77-*

536   *35*, MIT, Cambridge, MA.

537   Kausel, E., Whitman, A., Murray, J., and Elsabee, F. (1978). "The spring method for embedded

538   foundations," *Nuclear Engineering and Design*, 48, 377-392.

539   Kloukinas, P., Langoussis, M., and Mylonakis, G. (2012). "Simple wave solution for seismic

540   earth pressures on non-yielding walls," *J. Geotech. & Geoenv. Eng.*, ASCE, 138 (12), 1514–

541   1519.

542   Lew, M., Sitar, N. and Al-Atik, L. (2010). "Seismic earth pressures: Fact or fiction," in *Earth*

543   *Retention Conference 3*, ASCE Geotechnical Special Publication 208, R Finno, YMA Hashash,

544   and P Arduino (eds.).

545   Lysmer, J., Ostadan, F., and Chin, C. (1999). SASSI2000 *Theoretical Manual*, Geotechnical

546   Engineering Division, Civil Engineering Department, University of California, Berkeley.

547   Li, X. (1999). "Dynamic analysis of rigid walls considering flexible foundation." *J. Geotech.*

548   *Geoenviron. Eng.*, 125(9), 803-806.

549   Mononobe, N. and Matsuo, M. (1929). "On the determination of earth pressures during

550   earthquakes." *Proc. World Engrg. Congress*, 9, 179–187.

551   Mushkelishvili, N.I. (1963). "Some basic problems of the mathematical theory of elasticity." P.

552   Noordhoff, Groningen, The Netherlands. 714 p.

553   Mylonakis, G., Nikolaou, S., and Gazetas, G. (2006). "Footings under seismic loading: Analysis

554   and design issues with emphasis on bridge foundations," *Soil Dyn. Earthquake Eng.*, 26, 824-

555   853.

556   National Cooperative Highway Research Program, NCHRP (2008). *Seismic Analysis and Design*

557   *of Retaining Walls, Buried Structures, Slopes, and Embankments*. Report 611, Prepared by D.G.

558   Anderson, G.R. Martin, I.P. Lam, and J.N. Wang. Transportation Research Board, National

559   Academies, Washington DC.

560   National Institute of Standards and Technology, NIST (2012). *Soil-Structure Interaction for*

561   *Building Structures*, Report NIST GCR 12-917-21, Prepared by NEHRP Consultants Joint

562   Venture, J.P. Stewart, Project Technical Director. US Dept. of Commerce, Gaithersburg, MD.

563   Okabe, S. (1924). "General theory of earth pressure and seismic stability of retaining wall and

564   dam." *J. Japanese Society of Civil Engineering,* 12 (4), 34-41.

565   Ostadan, F. (2005). "Seismic soil pressure for building walls – an updated approach," *Soil Dyn.*

566   *Earthquake Eng.*, 25, 785-793.

567   Pais, A and Kausel, E. (1988). "Approximate formulas for dynamic stiffnesses of rigid

568   foundations," *Soil Dyn. Earthquake Eng.,* 7(4), 213-227.

569   Rathje, E.M., Faraj, F. Russell, S. and Bray, J.D. (2004). "Empirical relationships for frequency

570   content parameters of earthquake ground motions," *Earthquake Spectra*, 20 (1), 119-144.

571   Seed, H.B. and Whitman, R.V. (1970). "Design of earth retaining structures for dynamic loads."

572   *Proc., ASCE Specialty Conf. on Lateral Stresses in the Ground and Design of Earth Retaining*

573   *Structures*, Vol. 1, pp. 103-147, Cornell Univ., Ithaca, NY.

574   Steedman, R.S., and Zeng, X. (1990). "The influence of phase on the calculation of pseudo-static

575   earth pressure on a retaining wall." *Geotechnique*, 40(1), 103-112.

576   Trifunac, M.D., Todorovska, M.I., and Ivanović, S.S. (1996). "Peak velocities and peak surface

577   strains during Northridge, California, earthquake of 17 January 1994," *Soil Dyn. Earthquake*

578   *Eng.*, 15, 301-310.

579   Veletsos, A.S. and Prasad, A.M. (1989). "Seismic interaction of structures and soils: Stochastic

580   approach," *J. Struct. Engrg.,* 115 (4), 935–956.

581   Veletsos A.S. and Younan, A.H. (1994). "Dynamic soil pressures on rigid retaining walls."

582   *Earthquake Eng. Struct. Dyn.*, 23 (3), 275-301.

583   Wood, J.H. (1973). "Earthquake induced soil pressures on structures," *Report No. EERL 73-05*,

584   California Institute of Technology, Pasadena, CA.

585

586   **List of Figure Captions**

587   **Figure 1. Schematic illustration of the kinematic and inertial interaction components of foundation-**

588   **soil interaction for an embedded foundation system. FIM = Foundation Input Motion.**

589   **Figure 2. Schematic of embedded rigid strip foundation excited by vertically propagating shear wave.**

590   **Figure 3. Translational and rotational static stiffness interaction factors, χ_y and χ_{xx}, respectively,**

591   **versus H/B.**

592   **Figure 4. Normalized P_E versus normalized wavelength λ/H for various contributions of wall normal**

593   **stress to translational and rotational stiffness.**

594   **Figure 5. Kinematic transfer functions for translational and rotational Foundation Input Motions**

595   **derived from the present study and compared to the simplified approach of Kausel et al. (1978).**

596   **Figure 6. Maximum seismic earth pressure increments computed by Ostadan (2005) and Al Atik and**

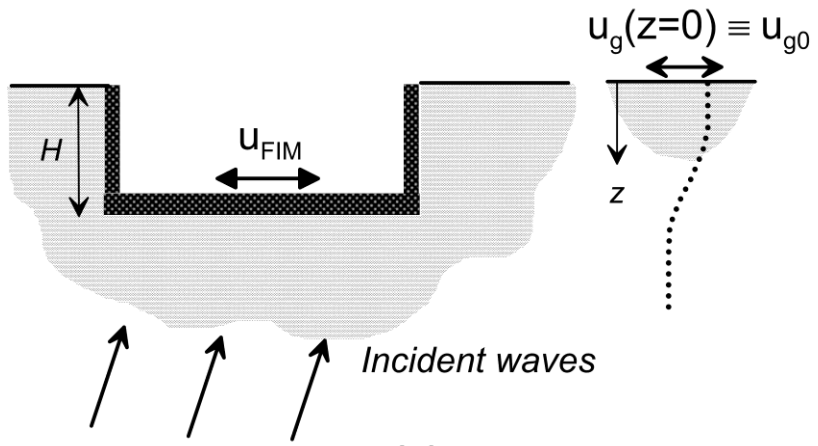597   **Sitar (2009) compared with full frequency-domain solution by the proposed kinematic methodology.**

598

599 **Table 1. Resultants of seismic earth pressure increments from Ostadan (2005), the Mononobe-Okabe**
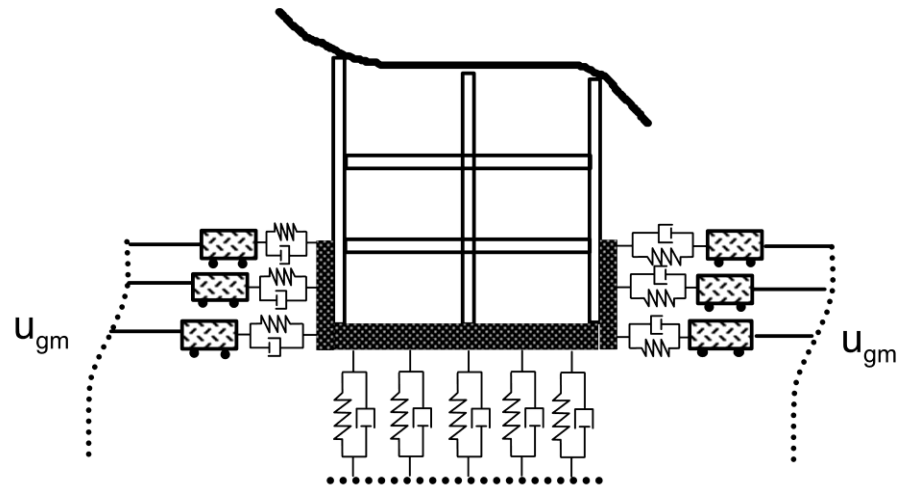
600 **solution, and the proposed kinematic methodology.**

	Earth Pressure Resultant, P_E (kN/m)			
Ground Motion	Ostadan (2005)	FD solution	SF solution	Mononobe-Okabe Solution
Loma Prieta	414	415 (+0%)	487 (+18%)	160 (-61%)
ATC	368	341 (-7%)	461 (+25%)	160 (-57%)
RG1.60	478	451 (-6%)	588 (+23%)	160 (-67%)
EUS distant	405	362 (-11%)	637 (+57%)	160 (-60%)
EUS local	179	201 (+12%)	158 (-12%)	160 (-11%)

601

602 **Table 2. Resultant of seismic earth pressure increments from Al Atik and Sitar (2009), the Mononobe-**

603 **Okabe solution, and the proposed kinematic methodology.**

	Earth Pressure Resultant, P_E (kN/m), (% error)			
Ground Motion	Al Atik and Sitar (2009)	FD solution	SF solution	Mononobe-Okabe solution
Loma Prieta SC1	90	110 (+23%)	95 (+6%)	180 (+100%)
Kobe PI2	146	164 (+13%)	180 (+23%)	∞ (+∞%)[1]
Loma Prieta SC2	101	94 (-7%)	121 (+20%)	235 (+132%)

604 [1] The M-O prediction of infinite earth pressure is caused by the inertial force exceeding the shear

605 strength of the sand at the base of the wall, and is a well-recognized unrealistic artifact that makes the

606 M-O theory difficult to apply in practice for sites with very strong design ground motions.
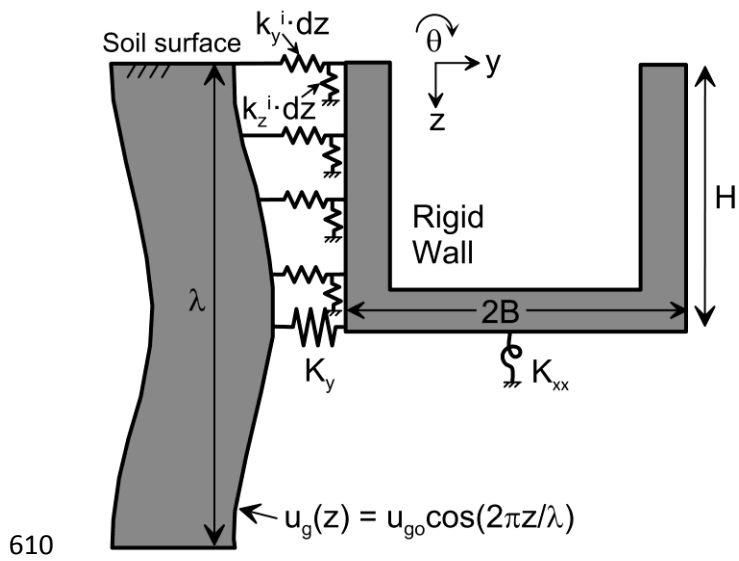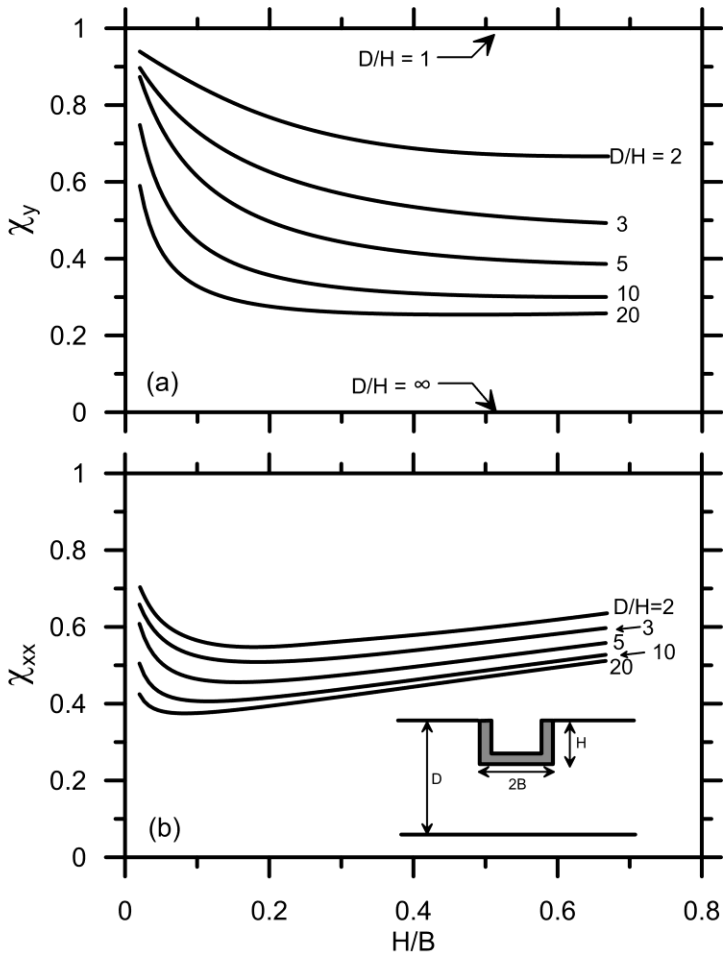
607

$u_g(z=0) \equiv u_{g0}$

u_{FIM}

H

z

Incident waves

(a)

u_{gm}

u_{gm}

(b)

608
609   Figure 1

Soil surface

$k_y^i \cdot dz$

$k_z^i \cdot dz$

θ

y

z

Rigid Wall

H

λ

2B

K_y

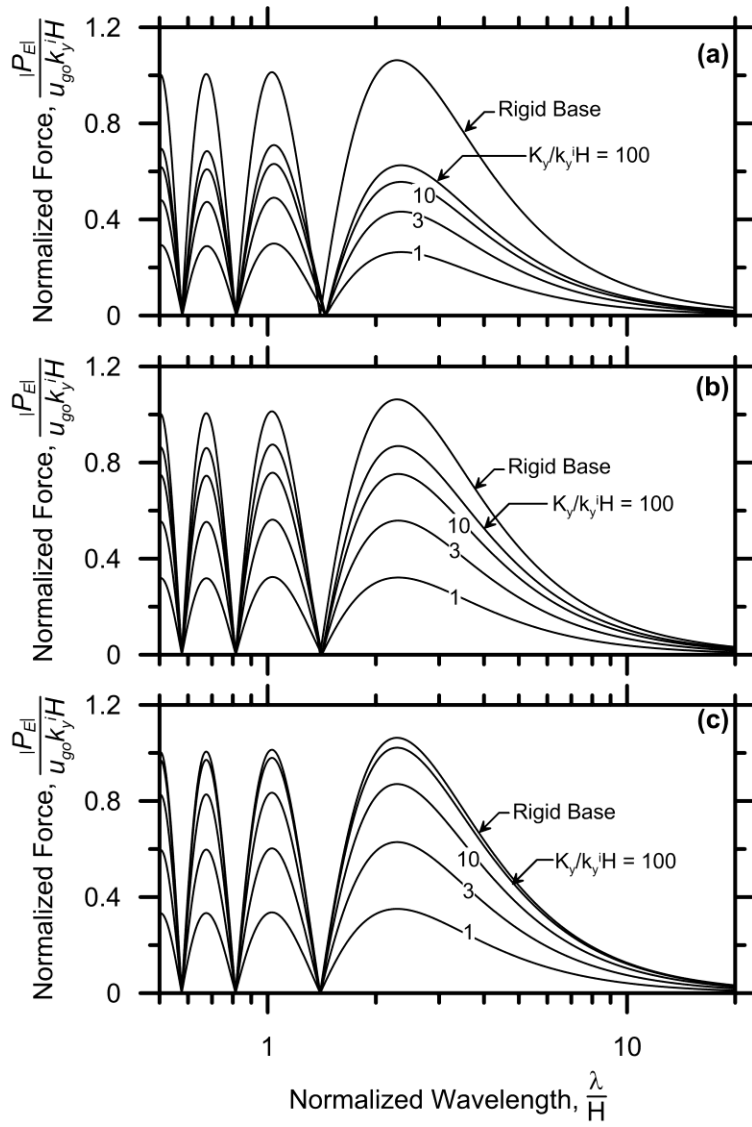K_{xx}

$u_g(z) = u_{go}\cos(2\pi z/\lambda)$
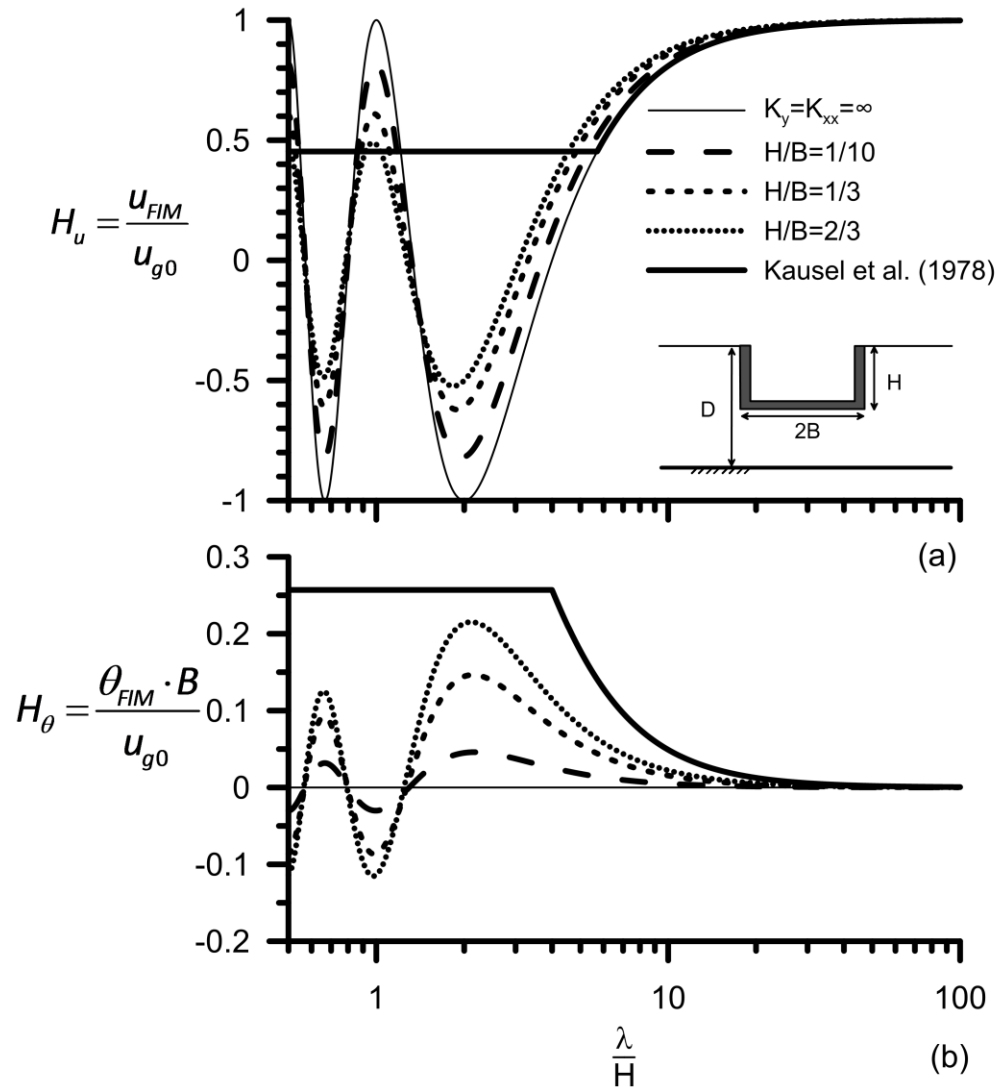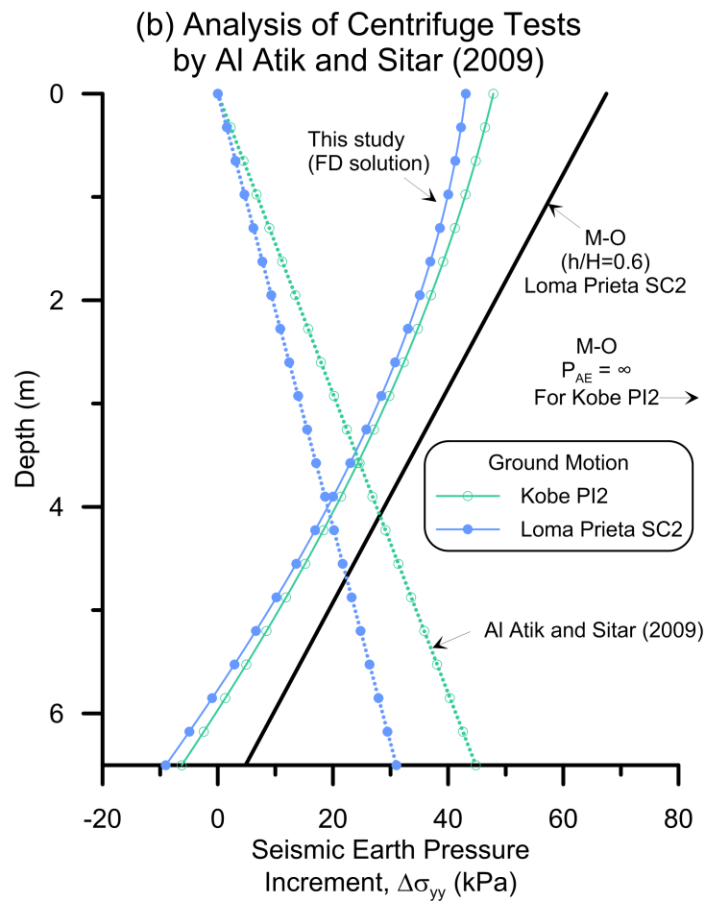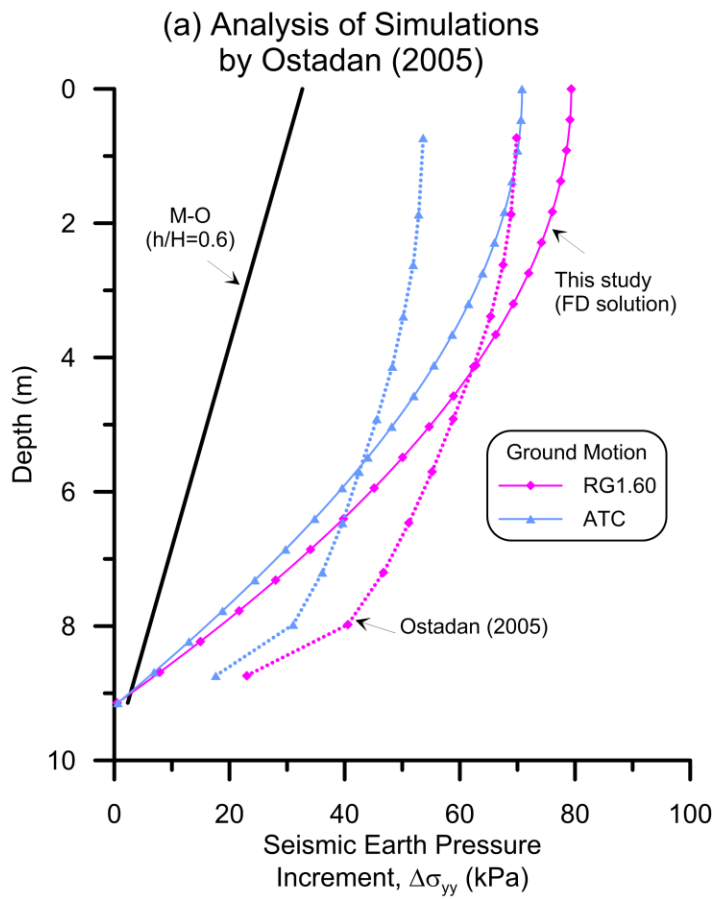
610

611   Figure 2

612

613

614   Figure 3

615

616   Figure 4

617

618   Figure 5

619

620   Figure 6

621 **Derivation of equation for vertical stiffness intensity $k_z{}^i$**

622   This digital supplement presents the derivation for vertical stiffness intensity, $k_z{}^i$, for an elastic soil
623   mass moving vertically relative to a rigid wall. The formulation follows the approach presented by
624   Kloukinas et al. (2012) for solving $k_y{}^i$ using a special integration technique inspired by the work of Vlasov
625   and Leontiev (1966). The solution procedure assumes that the free-field soil is vibrating according to a
626   vertical displacement field, and a vertical rigid wall alters the displacement field thereby mobilizing
627   shear tractions at the interface between the wall and the retained soil. The free-field vertical
628   displacement field is assumed to be known, and the horizontal variation in the vertical displacement
629   field caused by the presence of the rigid wall is subsequently solved to render vertical force equilibrium.

630   Stresses shown on the hatched region in Fig. 7 represent dynamic stress increments, and we
631   assume, following several related studies discussed in Kloukinas et al. (2012), that dynamic stresses in
632   the horizontal direction are zero (i.e., $\sigma_y = 0$) throughout the domain, plane-strain conditions apply, and
633   the displacement gradient $\dfrac{\partial u_y}{\partial z}$ is small compared to the complementary term $\dfrac{\partial u_z}{\partial y}$.

634   Equilibrium of vertical forces on the hatched region results in Eq. (A1).

$$\frac{\partial \sigma_z}{\partial z} + \frac{\partial \tau_{yz}}{\partial y} + \rho \frac{\partial^2 u_z}{\partial t^2} = 0 \tag{A1}$$

635

636   Stress-strain relations are provided in Eqs. (A2), in which G is shear modulus, and ν is Poisson ratio.

$$\sigma_z = -2G\left(\frac{\nu}{1-2\nu}\right)\frac{\partial u_y}{\partial y} - 2G\left(\frac{1-\nu}{1-2\nu}\right)\frac{\partial u_z}{\partial z} \tag{A2a}$$

$$\sigma_y = -2G\left(\frac{1-\nu}{1-2\nu}\right)\frac{\partial u_y}{\partial y} - 2G\left(\frac{\nu}{1-2\nu}\right)\frac{\partial u_z}{\partial z} \tag{A2b}$$

$$\tau_{yz} = -G\left(\frac{\partial u_y}{\partial z} + \frac{\partial u_z}{\partial y}\right) \tag{A2c}$$

637

638   By setting $\sigma_y = 0$, the y-direction displacement gradient can be expressed in terms of the vertical
639   displacement gradient and ν, as shown in Eq. (A3).

$$\frac{\partial u_y}{\partial y} = -\frac{\nu}{1-\nu}\frac{\partial u_z}{\partial z} \tag{A3}$$

640

641   After substituting Eq. (A3) into Eq. (A2a) and taking the partial derivative with respect to z, taking the

642   partial derivative of Eq. (A2c) with respect to y, and substituting into Eq. (A1) considering that $\dfrac{\partial u_y}{\partial z}=0$,

643   one obtains the governing equation

$$\psi_s^2 \frac{\partial^2 u_z}{\partial z^2}+\frac{\partial^2 u_z}{\partial y^2}+k^2\frac{\partial^2 u_z}{\partial t^2}=0 \tag{A4}$$

644

645   where $\psi_s=\sqrt{\dfrac{2-v}{1-v}}$ is a compressibility coefficient, and $k = \omega/V_s$ = wave number.

646

647   Following Kloukinas et al. (2012), we assume that the displacement field in the soil behind the

648   wall can be written in separable form

$$u_z(y,z)=Y(y)\Phi(z) \tag{A5}$$

649

650   where Y is an unknown function of the horizontal variable y, and $\Phi(z)$ is a predetermined dimensionless

651   function of the vertical variable that satisfies the geometric boundary condition $\Phi(H)$=0 and $\Phi(0)$=1.

652   To eliminate the variable z, Eq. (A4) is multiplied by $\Phi(z)$ and integrated over layer thickness to give

$$\psi_s^2 Y\int_0^H \frac{d^2\Phi}{dz^2}\Phi dz+\frac{d^2Y}{dy^2}\int_0^H \Phi^2 dz+k^2 Y\int_0^H \Phi^2 dz=0 \tag{A6}$$

653

654   The first term on the left hand side of Eq. (A6) can be integrated by parts to obtain the weak form

$$\psi_s^2 Y\int_0^H \frac{d^2\Phi}{dz^2}\Phi dz=\psi_s^2 Y\frac{d\Phi}{dz}\Phi\Big|_0^H -\psi_s^2 Y\int_0^H \left(\frac{d\Phi}{dz}\right)^2 dz \tag{A7}$$

655

656   Assuming a traction-free boundary condition at the soil surface means that $\dfrac{d\Phi}{dz}\Big|_{z=0}=0$. Combined with

657   the condition that $\Phi(H)$=0, the first term on the right-hand side of Eq. (A7) must also be zero. By making

658   appropriate substitutions and re-arranging terms, Eq. (A6) can be expressed as

$$\frac{d^2Y}{dy^2} - \left(\psi_s^{\ 2} \frac{\int_0^H \left(\frac{d\Phi}{dz} \right)^2 dz}{\int_0^H \Phi^2 dz} - k^2 \right) Y = 0 \qquad \text{(A8)}$$

659

660   The general form to the solution of Eq. (A8) is

$$Y(y) = C_1 e^{y\sqrt{a_c^2 - k^2}} + C_2 e^{-y\sqrt{a_c^2 - k^2}} \qquad \text{(A9)}$$

661

662   where $a_c^2 = \psi_s^{\ 2} \dfrac{\int_0^H \left(\frac{d\Phi}{dz} \right)^2 dz}{\int_0^H \Phi^2 dz}$.

663   Noting that Y(∞) is finite and Y(0) = u_o, one obtains C_1 = 0 and C_2 = u_o. Substitution into Eq. (A5) results in

$$u_z(y,z) = u_o e^{-y\sqrt{a_c^2 - k^2}} \Phi(z) \qquad \text{(A10)}$$

664

665   Substituting Eq. (A10) into Eq. (A2c), the expression for shear stress is

$$\tau_{yz}(y,z) = -G\frac{\partial u_z}{\partial y} = Ga_c e^{-y\sqrt{a_c^2 - k^2}} u_o \Phi(z) \qquad \text{(A11)}$$

666

667   The vertical stiffness intensity can then be computed as

$$k_z^i = \frac{\int_0^H \tau_{yz}(y,z)dz}{\int_0^H u_z(y,z)} = \frac{u_o G \sqrt{a_c^2 - k^2} e^{-y\sqrt{a_c^2 - k^2}} \int_0^H \Phi(z)dz}{u_o e^{-y\sqrt{a_c^2 - k^2}} \int_0^H \Phi(z)dz} = Ga_c \sqrt{1 - \left(\frac{k}{a_c} \right)^2} \qquad \text{(A12)}$$

668

669   Selecting $\Phi(z) = \cos\left(\dfrac{\pi z}{2H} \right)$, the value of a_c can be solved as:

$$a_c = \psi_s \left(\frac{\int_0^H \frac{d^2}{dz^2} \cos\left(\frac{\pi z}{2H}\right) dz}{\int_0^H \cos\left(\frac{\pi z}{2H}\right)^2 dz} \right)^{0.5} = \sqrt{\frac{2-v}{1-v}} \frac{\pi}{2H}$$ (A13)

670

671   Substituting Eq. (A13) into Eq. (A12) results in the final expression for k_z^i shown in Eq. (A14) and (7b)
672   from the main text.

$$k_z^i = \frac{\pi}{2} \sqrt{\frac{2-v}{1-v}} \frac{G}{H} \sqrt{1 - \left(\frac{2\omega H}{\pi V_s}\right)^2}$$ (A14)

673

674   Material damping can be incorporated into the solution for k_z^i by using the complex shear modulus,
675    $G(1+\mathbf{i}2\xi)$, where ξ is the percent damping. For static loading conditions in which $\omega = 0$, one obtains a
676   static stiffness shown in Eq. (A15). This equation may be appropriate when the loading frequency is
677   much lower than the natural frequency of the soil deposit.

$$k_z^i = \frac{\pi}{2} \sqrt{\frac{2-v}{1-v}} \frac{G}{H}$$ (A15)

678

679   Furthermore, as frequency becomes very high, the stiffness is complex due to the negative sign of the
680   quantity inside the square root in Eq. (A14), and the imaginary portion dominates and becomes equal to
681   Eq. (A16) as $\omega \to \infty$.

$$k_z^i = i\omega \frac{G}{V_s} \sqrt{\frac{2-v}{1-v}}$$ (A16)

682

683   This indicates that the wall stiffness can be represented by a dashpot c_z^i, in accordance with elementary
684   wave propagation theory (Eq. A17).

$$c_z^i = \rho V_s \sqrt{\frac{2-v}{1-v}}$$ (A17)

685

686　This suggests the existence of an equivalent propagation velocity, influenced by soil compressibility, in
687　accordance with Eq. (A4).
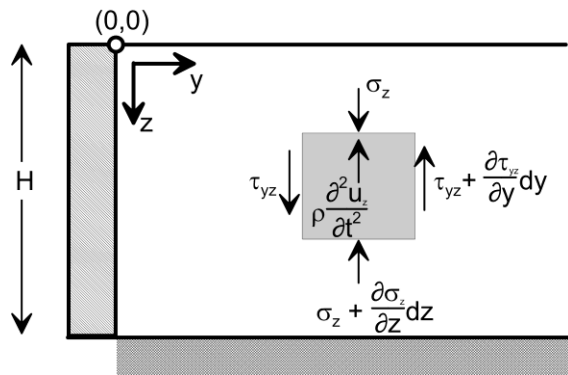
688　**References:**

689　Kloukinas, P., Langoussis, M. and Mylonakis, G. (2012). "Simple wave solution for seismic earth
690　pressures on non-yielding walls," *J. Geotech. & Geoenv. Eng.*, ASCE, 138 (12), 1514–1519.

691　Vlasov, V.Z. and Leontiev, U.N. (1966). *Beams, plates and shells on elastic foundation*, Israel Program for
692　Scientific Translation, Jerusalem (translated from Russian).

693　**List of Figure Captions:**

694　**Figure 7. Schematic of vertical wall and a soil element with vertical and shear stresses.**

695

696

697　Figure 7

698